Electrochemical conversion of CO_2 and CH_4 at subzero temperatures

Sargeant, Elizabeth; Kolodziej, Adam; Le Duff, Cecile; Rodriguez, Paramaconi

DOI:
10.1021/acscatal.0c01676

Document Version
Peer reviewed version

Citation for published version (Harvard):
Sargeant, E, Kolodziej, A, Le Duff, C & Rodriguez, P 2020, 'Electrochemical conversion of CO_2 and CH_4 at subzero temperatures', *ACS Catalysis*, vol. 10, no. 14, pp. 7464–7474. https://doi.org/10.1021/acscatal.0c01676

Electrochemical Conversion of CO_2 and CH_4 at Subzero Temperatures

Elizabeth Sargeant, Adam Kolodziej, Cécile S. Le Duff and Paramaconi Rodriguez*

School of Chemistry, University of Birmingham, Edgbaston, Birmingham B15 2TT

*Corresponding author: p.b.rodriguez@bham.ac.uk

Abstract

By taking advantage of the high solubility of CO_2 and CH_4 at low temperature, we report the electrochemical conversion of these gases in aqueous media down to -40 °C. The 5-fold increase in the concentration of CH_4 in gas hydrate slurries makes its electrochemical oxidation feasible at temperatures below the freezing point of water. We also report the electrochemical conversion of CO_2 at low temperatures and demonstrate, unexpectedly, that its reduction in these conditions follows an Anti-Arrhenius kinetics electrochemical environment. These findings open windows of investigations of electrocatalysis in brines below the freezing point of water.

Key words:

Electrocatalysis, CO_2 reduction, methane oxidation, brines, freezing point depletion, anti-Arrhenius

1. Introduction

Gas hydrates, or clathrates, were discovered in 1810 in the laboratory of Sir Humphrey Davy by cooling a solution saturated with chlorine gas below -9°C.[1] Since then, many other gas hydrates such as hydrates of hydrocarbons, sulfur dioxide (SO_2) and carbon dioxide (CO_2) have been discovered.[2,3] 200 years after the discovery of gas hydrates, they are barely used

and there are very few examples of technical applications.[4] In particular, these systems have been disregarded for electrocatalytic applications.

However, the recent discovery of perchlorate brines on Mars at the Phoenix landing site[5] has renewed interest in the scientific community in gas hydrates and the chemistry of brines. Given that the composition of the Martian atmosphere is 96 % CO_2 and, knowing the solubility of CO_2 increases with decreasing temperature, it is expected that such brines will have large amounts of carbonates and CO_2 hydrates.[6] Furthermore, the presence of CH_4 in the Martian atmosphere and formation of gas hydrates has recently been confirmed.[7]

NASA have continuously examined technologies that may enable Mars In-Situ Resource Utilization (ISRU).[8] Such technologies, should provide practical and affordable ways to use the local resources during the missions instead of the costly transportation of resources to Mars. The technologies should have the ability to transform the resources into air, fuels, water for drinking, fine chemicals, plant growth, rocket propellants, building materials, etc. CO_2 and CH_4 hydrates could be considered basic elements for human establishment as they could provide, directly or indirectly, fuel, water and standard industrial chemicals for the manufacture of plastics. In fact, the ISRU program has focused on the production of methane from atmospheric CO_2 and hydrogen brought from Earth via the Sabatier reaction, and the synthesis of oxygen required for propellant usage.[8]

Developing and understanding electrocatalytic reactions of gas hydrates at low temperature will be relevant for the development of technology capable of producing electricity by converting CH_4 into CO_2 and then recycling CO_2 back into CH_4. These reactions can then be used as a sustainable energy cycle, in a reversible fuel cell,[9] under severe environmental conditions. This will be critical to ensure the availability of key *in situ* resources sustaining future human exploration and colonisation of Mars, Figure 1. Such technology would be

based on reversible fuel cell/electrolyser technologies and preferentially taking place in water or gas hydrates.[10]

So far, electrocatalytic processes in aqueous solution have been extensively studied as a function of temperature in the range 0 to 99 °C but very little is known about electrocatalytic processes at temperatures below the freezing point of water or in gas hydrates.[11] The magnitude of freezing-point depression of the brine solution depends only on the solute concentration (*m*, molality) and the of number of ion particles per individual molecule of solute dissociated in the solvent (*i*, van 't Hoff coefficient). The magnitude of freezing-point depression can be estimated by the linear relationship of these two parameters and the cryoscopic constant (k_{freezing}):

$$\Delta T = imk_{\text{freezing}}$$

Decreasing the temperature of water to subfreezing temperatures significantly increases the solubility of gases in water,[12] and, as such, the reaction rate of the oxidation or reduction reaction can be increased. As the concentration of the gas increases, the chemical potential increases which might favour the adsorption of the reactive and intermediate species.

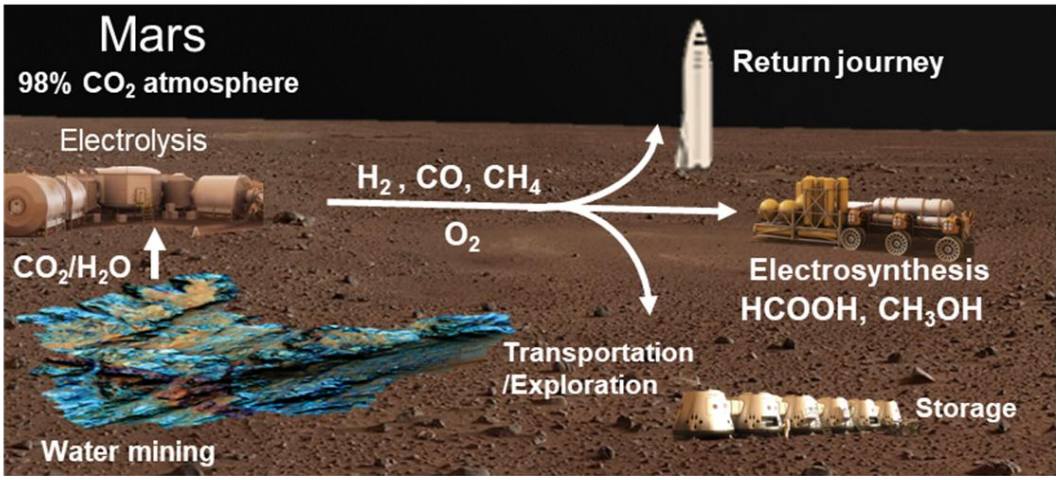

Figure 1. Electrochemical utilisation of CO_2 and methane transformation on Mars. The figure has been prepared based on the In situ Resource Utilization (ISRU) programme from NASA. Adapted from [13].

In this paper, we report the first electrochemical results for the oxidation of CH_4 and the reduction of CO_2 on platinum, palladium, gold and copper electrodes in aqueous brines at subfreezing temperatures, down to -38 °C. The systems were evaluated in different brines such as 4.4 m $Mg(ClO_4)_2$, similar to those brines observed on Mars, 11 m NaOH and 10 m KOH solutions.

2. Results and Discussion

2.1 Hydrogen UPD and hydrogen evolution reaction (HER) in brines

The current-potential curves (*I*-*V*) of Pt(111) and Pt(100) single-crystal electrodes in a 4.4 m $Mg(ClO_4)_2$ solution at different temperatures are shown in Figure 2A. Below 0.5 V vs. RHE the features are associated with the hydrogen adsorption/desorption process and at potentials higher than 0.5 V vs. RHE the features are due to the formation and reduction of the surface oxides. The so-called hydrogen UPD is reversible for both electrodes at room temperature and becomes irreversible when the temperature is decreased down to -18 °C. Similarly, the voltammetric features associated to the oxidation and reduction of the surface change significantly when the temperature is reduced from room temperature to -18 °C. Such irreversibility in the hydrogen UPD and the surface oxides processes are not due to the presence of any type of contamination present in the electrolyte but because larger overpotentials are required for processes to take place at lower temperature. The degree of cleanliness and the effect of the purity of the electrolyte are discussed in the supporting information, Figure S10.

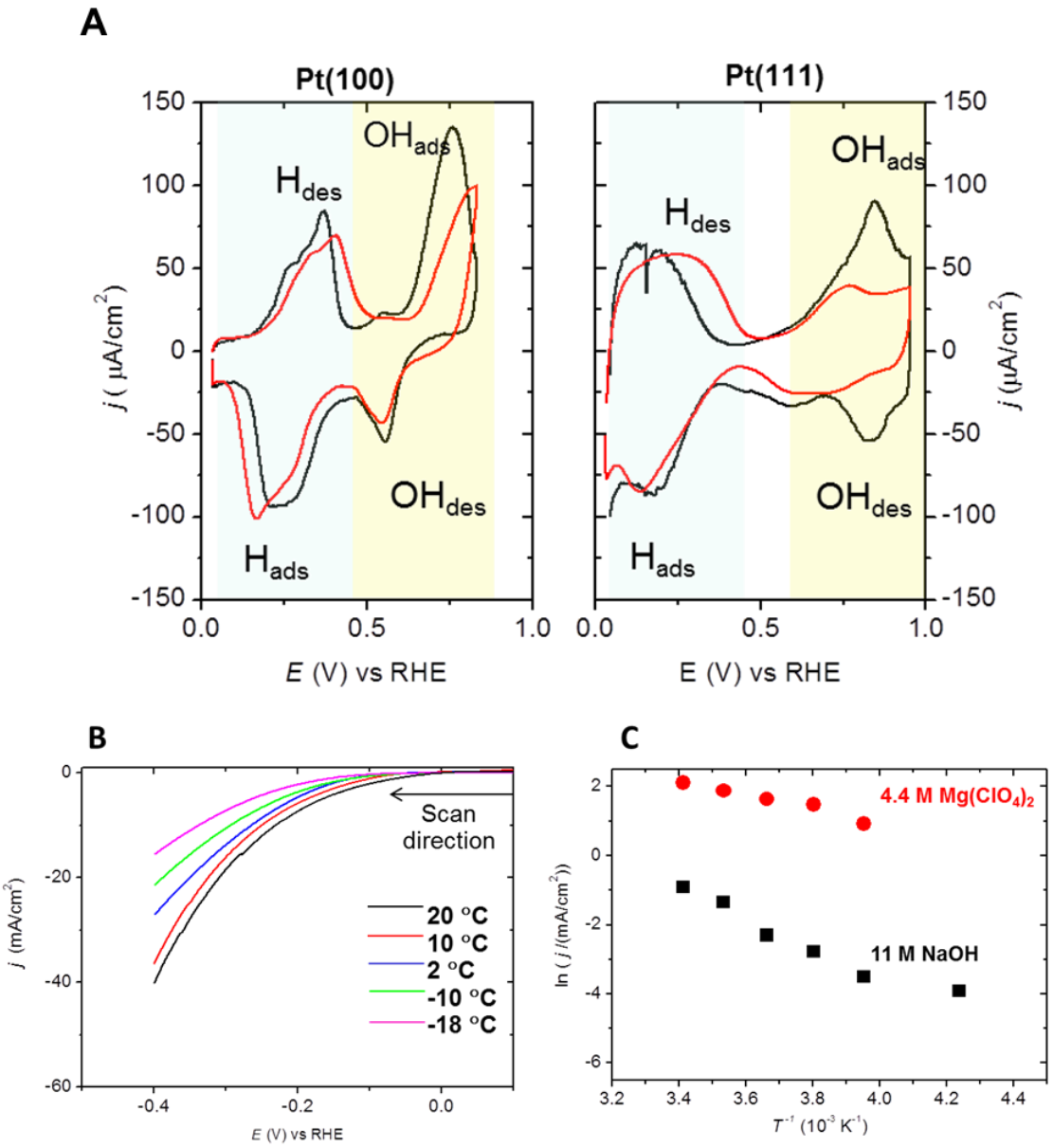

Figure 2. (A) Voltammetric profiles of Pt(100) and Pt(111) in 4.4 m solution of $Mg(ClO_4)_2$ at +20 °C (black curve) and -18 °C (red curve). (B) Voltammetric profiles of Pt(111) in 4.4 m $Mg(ClO_4)_2$, temperatures indicated in the figure. (C) Arrhenius plots for the HER on Pt(111) at -0.1 V vs RHE in 11 m NaOH and 4.4 m solution of $Mg(ClO_4)_2$.

The irreversibility of the hydrogen adsorption/desorption as a function of the temperature contrasts with previous results by Arvia *et al.* [11b, 14] in concentrated sulphuric and perchloric

acid. This can be attributed to the large difference in proton concentrations between the concentrated acid solutions and the $Mg(ClO_4)_2$ brines used in this work. For both electrodes, Pt(111) and Pt(100), the hydrogen desorption peak shifts to more positive potentials, 100 mV and 120 mV respectively, when the temperature decreases from 20 °C to -18 °C. In the same range of temperature, the hydrogen adsorption peak shifts to more negative potentials, 56 mV and 90 mV respectively. This corresponds to a temperature coefficient of approximately 2 mV K^{-1}, an average of the adsorption and desorption processes. This is larger than the calculated temperature coefficient of 0.65 mV K^{-1} for the reversible hydrogen electrode in 0.1 M H^+ solution[15] and the shift of 0.45 mV K^{-1} estimated from the adsorption isotherm of hydrogen on Pt(111) in 0.1 M $HClO_4$ by Markovic *et al.*[16] The variation can be attributed not only to differences in the proton concentration but also to the nature and concentration of the ions in solution as described by Debethune *et al.*[15] As a consequence of the shift in the hydrogen adsorption at low temperature, the onset of the hydrogen evolution reaction (HER) also shifts towards more negative potentials as shown in Figure 2B.

This is an important parameter to determine, as the HER is a competitive reaction during the electrochemical reduction of CO_2. Previous works by Frese *et al.*[17] showed that the HER on platinum electrodes at -45°C in $HClO_4.5.5H_2O$, close to the freezing point of the electrolyte, follows the Volmer-Tafel mechanism where the combination of two adsorbed hydrogen atoms to form H_2 is rate determining:

$H_{aq}^+ + e^- \Leftrightarrow H_{ad}$ (Volmer reaction)

$2H_{ad} \Leftrightarrow H_2$ (Tafel reaction, RDS)

In acidic media, the mechanism of HER is not dependent on the temperature as the Tafel slope is independent of T and a proton tunnelling mechanism has been proposed.[11a, 17] Our results show a Tafel slope of 40 mV dec^{-1} at 20 °C for the HER in 4.4 m solution of

$Mg(ClO_4)_2$. This indicates that either the Tafel step is the rate determining step or that the rate determining step is a chemical step preceded by a 2-electron transfer step. The chemical steps could be related to the reorganisation of the water molecules in the presence of a high concentration of ions. Unlike in acidic media, the HER in $Mg(ClO_4)_2$ showed changes in the Tafel slope as a function of the temperature, from 40 mV dec^{-1} at 20 °C to 65 mV dec^{-1} at -18 °C. This result is consistent with the expected short range structural rearrangement of water around both cations and anions.[18] In 11 m NaOH at 20 °C, a value of 135 mV dec^{-1} was found for the Tafel slope. This implies that the Volmer step, which is the first electron transfer, is the rate determining step:

$H_2O + e^- \Leftrightarrow H_{ads} + OH^-$ (Volmer step in alkaline media, RDS)

This is in agreement with previous results for the HER in alkaline media with much lower concentrations of hydroxide.[19] In acidic media, the anions occupy the large cavities in the water cage-like structure and the excess of delocalised protons act as charge carriers. In alkaline media, it is the cation that occupies the cavities of the water cage structure and the hydroxyl ions act as the charge carriers. Given the absence of free protons in alkaline solution, the protons for the hydrogen adsorption and HER come from the water molecules. It has been previously reported that water at the liquid/solid interface has a well-ordered structure which is lower in free energy than either ice or clathrate and higher in energy than liquid water under the same thermodynamic conditions.[20] This ordering increases on cooling, giving way to heterogeneous ice nucleation from the surfaces.[21] However, the water structure ordering results in a higher energy barrier that needs to be overcome for proton adsorption and subsequent HER.[20] The Tafel slopes in alkaline media are also temperature dependent,[18d, 22] increasing from 135 mV dec^{-1} at 20 °C up to 190 mV dec^{-1} at -35 °C. The decrease in catalytic activity as the temperature decreases follows an expected Arrhenius behaviour, as shown in Figure 2C. The apparent activation energies (E_a) in $Mg(ClO_4)_2$ and NaOH obtained

from the Arrhenius plots were 17.27 kJ mol^{-1} and 31.78 kJ mol^{-1}, respectively. Previous reports have shown E_a values for H on Pt electrodes in HCl/CH_3OH and 0.1 M KOH of 11.2 kJ mol^{-1} [11a] and 28.9 kJ mol^{-1} [19c] respectively. The differences in E_a can be partly attributed to the different pH values but are mainly due to the co-adsorption of cations (Na^+ vs Mg^{2+}).[23]

On palladium electrodes, in addition to the shift towards more negative potentials for the hydrogen adsorption/absorption process upon decreasing the temperature, the intensity of the peaks associated to the hydrogen oxidation also changed, Figure S11. This change is related to different rates of diffusion of the hydrogen through the two distinct palladium hydride phases, α- and β-, and the transformation between these phases.[24]

2.2.Electrochemical reduction of CO_2 in brines

Previous studies have shown that the changes in the lattice parameter of palladium and the hydrogen diffusion in the palladium structure influence the catalytic activity and selectivity of the electrochemical reduction of CO_2.[25] Therefore, it is expected that the changes to the absorption, diffusion and desorption of the hydrogen in the palladium electrodes and the increased concentration of CO_2 at low temperatures will strongly influence the electrochemical catalytic activity and selectivity of the reduction of CO_2.[26] As mentioned before, the HER competes with CO_2 reduction on some metal electrodes, such as copper and palladium. In gas hydrate crystal structures, the arrangement of their hydrogen bond network is “ice-like” but slightly more distorted. Due to the formation of the ice-like ordered structure of water, the HER might be hindered resulting in changes to the kinetics and selectivity of CO_2 reduction.[11b, 11d, 17]

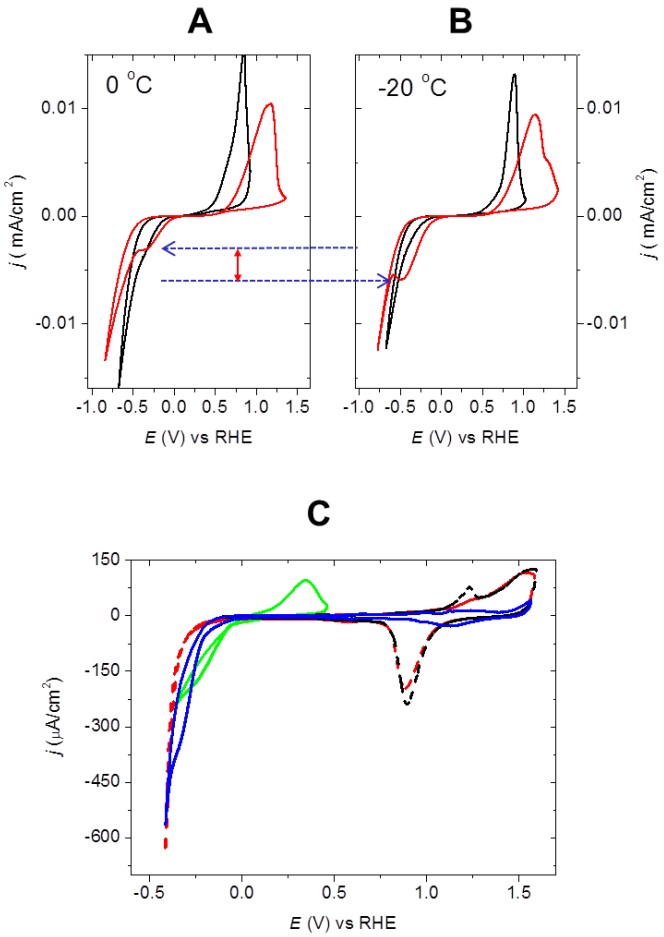

Figure 3. (A-B) Voltammetric profiles of a Pd polycrystalline electrode at 0 °C and -20 °C in an Ar-saturated solution of 10 m KOH (black curve) and in a CO_2-saturated solution of 10 m KOH (red curve) Scan rate, υ=50 mV/s. (C) Voltammetric profiles of Au polycrystalline electrode in a CO_2-saturated solution of 4.4 m $Mg(ClO_4)_2$ at 0 °C (red curve), -10 °C (blue curve) and -18 °C (green curve). The voltammetric profile of the gold electrode at 0°C in absence of CO_2 (black dashed curve) was included for comparison. Scan rate, υ=50 mV/s

Figures 3A and 3B shows the electrochemical reduction of CO_2 on palladium electrodes in a 10 m KOH solution at two different temperatures. It shows that, the CO_2 reduction, indicated by an arrow, is favourable at the lower temperature. Although seemingly counter intuitive, this behaviour can be attributed to the increase in the solubility of CO_2 due to the formation of

the water cages as the temperature decreases. As the concentration of CO_2 increases with decreasing temperature, the formation of carbonate species is favourable. Potassium was selected as the cation of choice over sodium because when NaOH was used a white precipitate of $NaHCO_3$ formed at low temperatures. The measured pH after CO_2 saturation at -18 °C was 11 which indicates the formation of carbonate/bicarbonate species. It is important to note that such species are present in the Mars atmosphere and determine the oxidation/reduction potential of the Martian soil.[6e] All the CO_2 reduction reaction curves were corrected for the corresponding change of the pH at each temperature on the RHE scale.

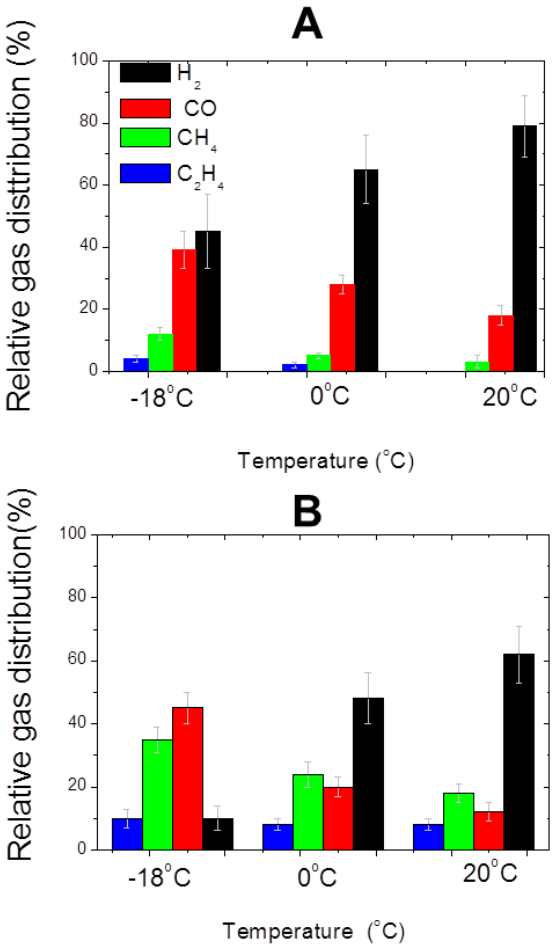

Figure 4. Gas product distribution during the CO_2 reduction on (A) Pd and (B) Cu electrodes after 15 minutes electrolysis at -0.6 V vs RHE in 4.4 m $Mg(ClO_4)_2$

Table 1. Summary of the liquid products identified after 20 min of electrolysis, at -0.6 V in a CO_2-saturated solution of 4.4 m $Mg(ClO_4)_2$ on Cu(111) and Pd(polycrystalline)

Electrode	Temperature (℃)	Species detected in the 1D ^{1}H spectrum	Species detected in the 1D ^{1}H-decoupled ^{13}C spectrum
Pd	20	HCOOH – trace	None detected (10,000 scans)
	-18	**HCOOH** – 0.30 mM EtOH – 0.06 mM	**$HCOO^-$**
Cu	20	**HCOOH** – 0.27 mM, EtOH – 0.02 mM	**$HCOO^-$** $CH_2(OH)_2$
	-18	**HCOOH** – 0.26 mM, **EtOH** – 0.13 mM, MeOH – trace	**$HCOO^-$** **EtOH** $CH_2(OH)_2$

*Species found in both types of spectra (^{1}H and ^{13}C) are highlighted in bold.

The product distribution for this reaction was followed by On-line Electrochemical Mass Spectrometry (Figure S1) and NMR (Table 1 and Figure S4-8). As can be seen in Figure 4A, the formation of hydrogen decreases when decreasing the temperature from 20 °C to -18 °C. At the same time, a small increase in the formation of other hydrocarbons was observed as the temperature decreased. It has been previously reported that the electrochemical reduction of CO_2 results in the formation of formic acid (formate) at low overpotentials.[25b] At this pH and temperature, the formate is not volatile and its detection was not possible by OLEMS. The formation of other gases, such as CO and other hydrocarbon species (C_xH_y), also increased upon decreasing the temperature. The liquid products were identified and quantified using water suppression NMR, Table 1.[27] The NMR spectra, Figure S6, show the different selectivity of the reduction of CO_2 at different temperatures. At the lower temperature, the formation of formic acid is enhanced and ethanol, which is not observed at 20°C, is formed. Previous works have reported the formation of H_2, CO and formic acid as the main products of the electrochemical reduction of CO_2 on Pd.[25b, 28] Here for the first time, we report the formation of ethanol as one of the products of the reduction of CO_2. We believe

that the C-C coupling is promoted by the increase of the surface coverage of CO at low temperatures and the change of the lattice of the palladium.

Figure 3C shows the electrochemical reduction of CO_2 on Au(111) electrodes in 4.4 m $Mg(ClO_4)_2$ at 0°C and -18 °C. As in the case of Pd and Pt, the electrochemical reduction of CO_2 is favoured at lower temperatures. Interestingly, the voltammetric profile at -18 °C showed an oxidation signal at 0.4 V vs RHE which is not present at 0 °C. Since the main product of the CO_2 reduction on gold is CO, this signal is likely due to the oxidation of CO. Earlier work has shown that CO oxidation takes place on gold electrodes at lower potentials in alkaline media.[29] As the CO_2 reduction reaction takes place, the local pH becomes more alkaline due to the HER favouring the adsorption and oxidation of CO. However, such an effect should also be observed at 20 °C. The presence of the signal only at low temperature can be attributed to the higher concentration of CO near the electrode at low temperature, resulting from the increased CO_2 reduction reaction.

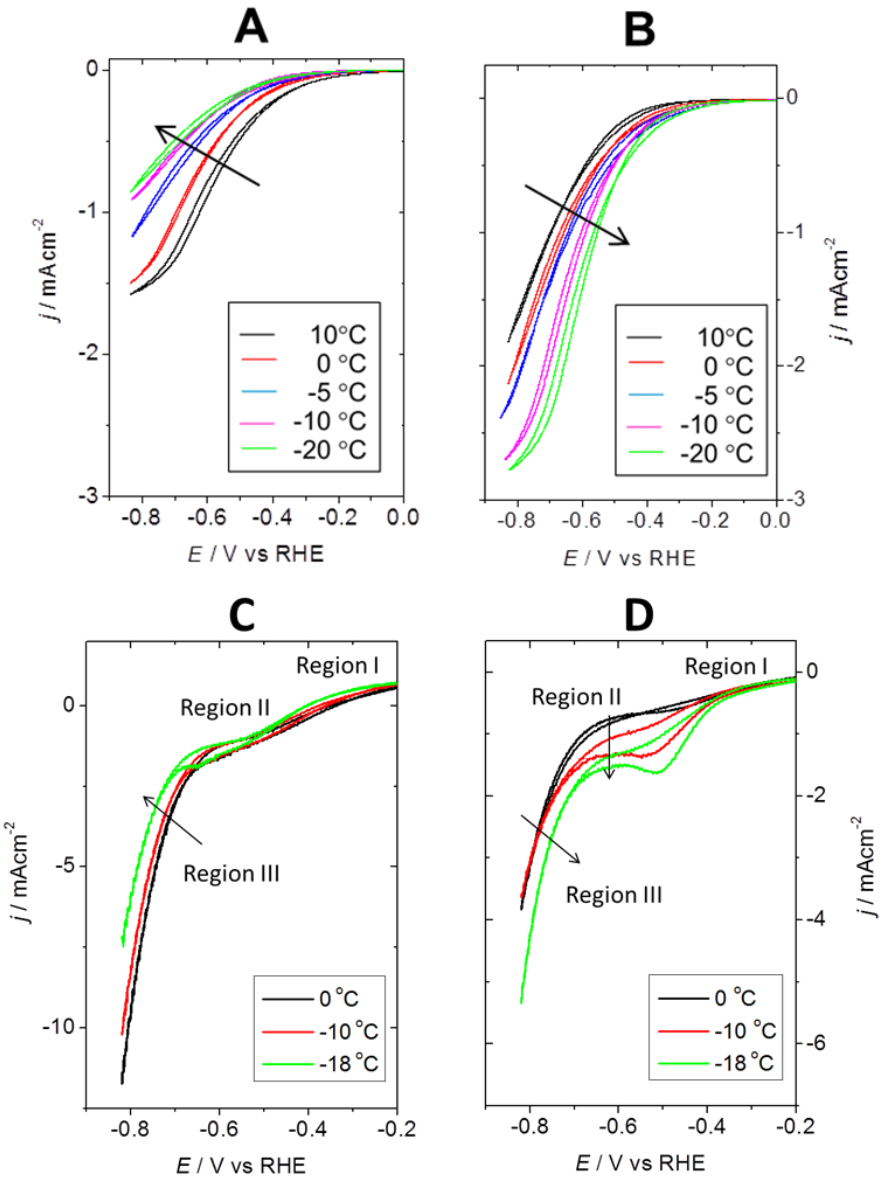

Figure 5. (A-B) Voltammetric profiles of Cu(111) electrode in (A) Ar-saturated and (B) CO_2 saturated 4.4 m $Mg(ClO_4)_2$. The solutions were saturated and the voltammetries were recorded with a stationary electrode and at different temperatures as indicated in the figure. The arrow indicates the trend as a function of the temperature. (C-D) HMRDE voltammograms of Cu(111) electrode in a (C) Ar-saturated and (D) CO_2-saturated solution of 4.4 m $Mg(ClO_4)_2$ at different temperatures. Rotation rate: 1600 RPM and scan rate, υ=: 50 mV s^{-1}. The arrow indicates the trend as a function of the temperature.

The curves for the electrochemical reduction of CO_2 on Cu(111) in static conditions, as a function of the temperature, are shown in Figures 5A and 5B. It was found that the currents associated to the CO_2 reduction increased as the temperature decreased, likely due to the increase of the concentration of CO_2 in solution.

It is well known that mass transport gradients play an important role in the kinetics of the CO_2 reduction reaction and HER. The use of a hanging-meniscus rotating electrode during experiments on the Cu(111) enable strict control over the mass transport, diminishing the concentration gradients at the electrode interface, and by minimising changes of the pH at the surface.

Figures 5C and 5D show cyclic voltammograms of a Cu(111) rotating disc electrode in a hanging meniscus configuration (HMRDE) in Ar-saturated and CO-saturated 4.4 m $Mg(ClO_4)_2$ electrolyte at different temperatures. Three well defined regions can be distinguished. In the Figure 5C, Ar-saturated solution, region I, between -0.2 V and -0.45 V vs RHE is assigned to hydrogen evolution reaction from proton reduction. Region II, between -0.45 V and -0.7 V vs RHE leads to a current plateau indicating mass transport limitation. In region III, at potentials more negative than -0.7 V RHE, the current increases independently from proton mass transport and can be assigned to HER from water reduction.

As can be seen in Figure 5C, Ar-saturated solution, the onset of the proton reduction current in region I, is slightly shifted to a more negative potential and the diffusion current, region II, is almost unaltered when the temperature is decreased from 0 to -18 °C. This is an indication that the mass transport and reduction of protons is almost independent of the temperature. On the other hand, the HER from water reduction, region III, is shifted to more negative potentials as the temperature decreases. Interestingly, the larger overpotential was found at -18°C where the crystallization of the water is expected at this concentration of the brine.

In contrast, the CO_2-saturated solution, Figure 5D, the voltammograms are strongly influenced by the temperature. The onset potentials in regions I and III, shift towards more positive potentials and the diffusion limiting currents increase as the temperature decreases. These results show that under well-defined mass transport conditions, the rate of the reduction of CO_2 is largely dependent on temperature and that the concentration of CO_2 at the interface is greater at low temperatures as confirmed in Figure S3.

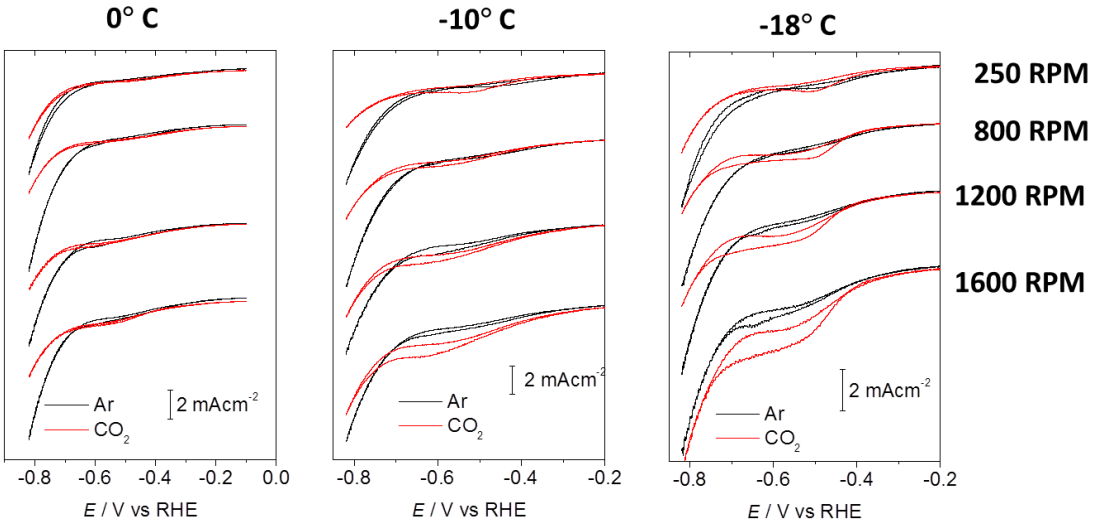

Figure 6. HMRDE voltammograms of Cu(111) electrode in (black curve) Ar-saturated (red curve) CO_2-saturated solution of 4.4 m $Mg(ClO_4)_2$ at different temperatures and rotation rate as indicated in the figure. Scan rate, 50 mV s^{-1}.

Figure 6 shows the comparison between the voltammograms of Cu(111) HMRDE in an Ar-saturated and CO_2-saturated 4.4 m $Mg(ClO_4)_2$ electrolyte at different temperatures and different rotation rates.

Compared to the Ar-saturated solution, at temperatures above -10 °C the onset of reduction current in the CO_2-saturated solution in region III, is slightly shifted to a more negative potential. However, as the temperature becomes more negative and the rotation rate increases, the onset of the reduction current shifts to more positive potentials. It is also important to note, at temperatures greater than 0 °C the diffusion current, region II, is almost

identical to the diffusion current in Ar-saturated electrolyte, independent of the rotation rate as previously reported for the reduction of CO_2 in acidic media.[30] This is in contrast to lower temperatures, -10 °C to -18 °C, where the diffusion current increases as the rotation rate increases. Since the diffusion current, from the Levich constant depends on the kinematic viscosity ($\upsilon^{-1/6}$) and the diffusion coefficient ($D^{2/3}$), where both factors decrease with temperature, the only possible factors that might result in an increase in the diffusion current are the number of electrons (n) and the concentration (C). It was previously proven that the concentration of CO_2 increased with decreasing temperature, Figure S3. Below, we will discuss the changes in the product selectivity that result from the change in the number of electrons transferred. The increase in the limiting current, as a function of the rotation rate, at -18 °C might also influence the onset of the reduction current in region III.

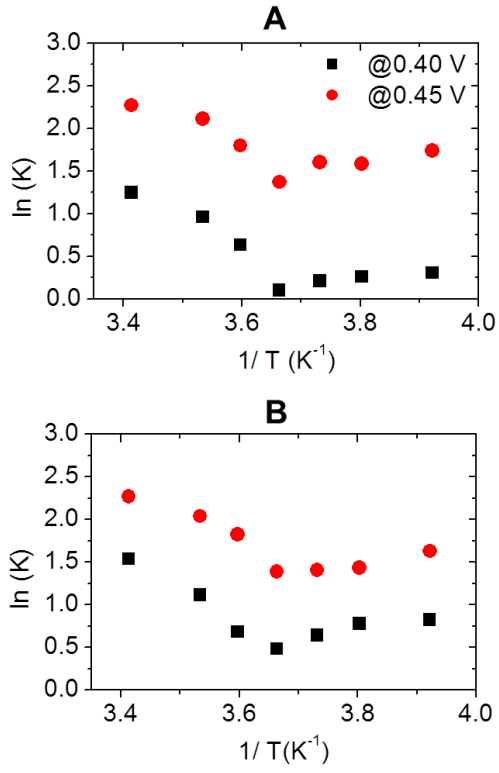

Figure 7. Arrhenius plots at -0.4 V (black square) and -0.45 V (red circle) on a Cu(111) electrode in a CO_2-saturated solution of 4.4 m $Mg(ClO_4)_2$. To obtain the ln(*K*) the

kinetic currents (j_k) at each potential were corrected by the diffusion current (j_d) at -0.72 V according to the modified Koutecky-Levich equation.(A) Currents obtained at 250 rpm and (B) currents obtained at 1600 RPM

In order to determine the E_a of the process from the Arrhenius plots, the true kinetic currents (j_{kin}) were determined at -0.4 V and -0.45 V vs RHE by correcting the currents at each potential (j) by the diffusion currents (j_{Diff}) using the modified Koutecký–Levich equation as previously described for the ORR.[31] The concentration of the CO_2/HCO_3^- was also determined at each temperature following the procedure described in the SI and shown in Figure S2. Figure S3 shows how the solubility of CO_2 increases as the temperature decreases. As a result of the increase in the solubility of CO_2, HCO_3^- is formed and the pH increases. The Arrhenius plots for the Cu(111) electrode at 2 different potentials, -0.4 V vs RHE, region I, and -0.45 V vs RHE, region II, and 2 rotation rates are shown in Figure 7. The kinetic constants were determined, taking into account that both CO_2 and HCO_3^- are reactive species in the CO_2 reduction reaction. As can be seen, the Arrhenius plots present two different slopes, positive slopes at temperatures greater than -5°C and negative slopes at temperatures less -5°C, independent of rotation rate and the potential. At higher temperatures, greater than -5°C, the calculated E_a values were E_a = 4.3 ± 0.3 kJmol^{-1} at -0.4 V and E_a = 3.58±0.04 kJmol^{-1} at -0.45 V and at temperatures lower than -5°C, the Arrhenius plots show an Anti-Arrhenius behaviour with E_a = -1.25±0.25 kJmol^{-1} at -0.4V and E_a = -1.52±0.08 kJmol^{-1} at -0.45 V.

Other kinetic parameters, such as Tafel plots and the electron transfer coefficient, could be extracted from the cyclic voltammetry, however this manuscript does not include the kinetic analysis to avoid oversimplifying of the process. Previous works have oversimplified the analysis of the kinetics of the CO_2 reduction reaction, typically assuming that the surface coverage of the intermediate species is constant.[32] However, this simplification leads to an

incomplete description of the actual surface kinetics, in particular on Cu electrodes where the coverage of different reaction products and different intermediate adsorbed species varies with the applied potential.

Regarding the selectivity, results seen in Figure 4B, show that on Cu(111) the HER decreases and the formation of hydrocarbons, CH_4 and C_2H_4, increases as the temperature decreases from 20 °C to -18 °C. Similar trends were observed by Ahn *et al.* for the temperature range between 42 °C and 2 °C.[33] An increase in the CO production rate was also observed at low temperatures. It is important to note that the solubility of all these gases, CH_4, C_2H_4 and CO, increase at low temperature due to the formation of their respective gas hydrates. The NMR analysis, Table 1, shows larger concentrations of formic acid and small amounts of methanol, gem-diol and ethanol were detected after 20 min of electrolysis at -18 °C.

The changes in product selectivity during the CO_2RR can be attributed to different sources, and in fact many of the reasons can be interlinked. As shown before, the decrease in the temperature results in a decrease of the HER, but also result in an increase of the solubility of the CO_2 species. Koper's group reported that the water reduction pathway is specifically inhibited by adsorbed CO during the CO_2RR leading to high faradaic efficiency for CO_2 reduction on copper electrodes. This inhibition of the HER pathway becomes more pronounced at increased mass transport of CO_2.[30] In our system, the mass transport is not only affected by the decrease in the temperature but also by the viscosity of the highly concentrated electrolyte. Jaramillo's group reported that methane formation only occurs at potentials within a CO mass-transport-limited regime and the C2+ products are sensitive to the CO partial pressure.[34] While the mass transport effect has been mainly identified on high-surface area nanostructured electrodes,[35] based on the results on HMRDE , mass transport effects on the product selectivity in our extended surface electrodes cannot be discarded. In

addition, the solvation of the CO_2 and the intermediates by a more rigid structure of the water in the CO_2 hydrate might affect the product selectivity.

Previous works have demonstrated that in gas hydrate crystal structures, the arrangement of their hydrogen bond network is "ice-like" but with slight distortions. Further stabilized by encaging a guest molecule, the cage structures in gas hydrate crystals are considered relatively rigid and the lattice water molecules are largely restricted from rotation and translation [36]The rigidity of the gas hydrate structure may influence different steps of the reaction mechanism. Studies performed by Luo *et al.* suggest that the hydrogenation of CO_{ads} to COH_{ads} or CHO_{ads} is a key step determining the selectivity of the reduction of CO_2 to hydrocarbons.[37] The formation of these intermediates depends on the coverage of CO and protons, which depends on the applied potential.

2.3. Electrochemical oxidation of CH_4 in brines at -40°C.

As previously mentioned, another interesting system to study is the electrochemistry of methane hydrates due to their abundance in deep ocean sediments and as icy brines on Mars.[38] Figure 8A shows the concentration of CH_4 in H_2O and 11 m NaOH as the temperature decreases. The concentration of CH_4 in water at temperatures between 20°C and 0°C are in agreement with previous values reported.[12, 39] It was found that the concentration of CH_4 decreases upon increasing the salinity of the solution.[39] However, by increasing the concentration of NaOH, lower temperatures can be reached so there is a net increase in CH_4 solubility at the lowest temperature of -38°C. Upon bubbling CH_4 through an 11 m NaOH solution at -38 °C, the solution turned into a viscous emulsion-slurry solution[40] Figure 8B. The voltammetric profile of Pt(111) in this solution is shown in Figure 8C. At this temperature, an oxidation wave is observed in the positive scan between 0.4 and 0.6 V vs RHE, confirming the oxidation of CH_4. At higher potentials the platinum oxide features are

smaller than those in a solution without CH_4. This suggests the presence of adsorbed intermediate species, which are products of the oxidation of methane at lower potentials. The broadening of the double layer and the reduction currents in the negative going scan also suggest the presence of adsorbed intermediate species. At 20 °C under the same conditions of electrolyte concentration, the platinum electrode did not show any signal associated with the oxidation of CH_4. This is also true for temperatures ranging between 20°C and -30°C. The oxidation of methane was only observed between -30°C and -38°C upon the formation of the gel or slurry.

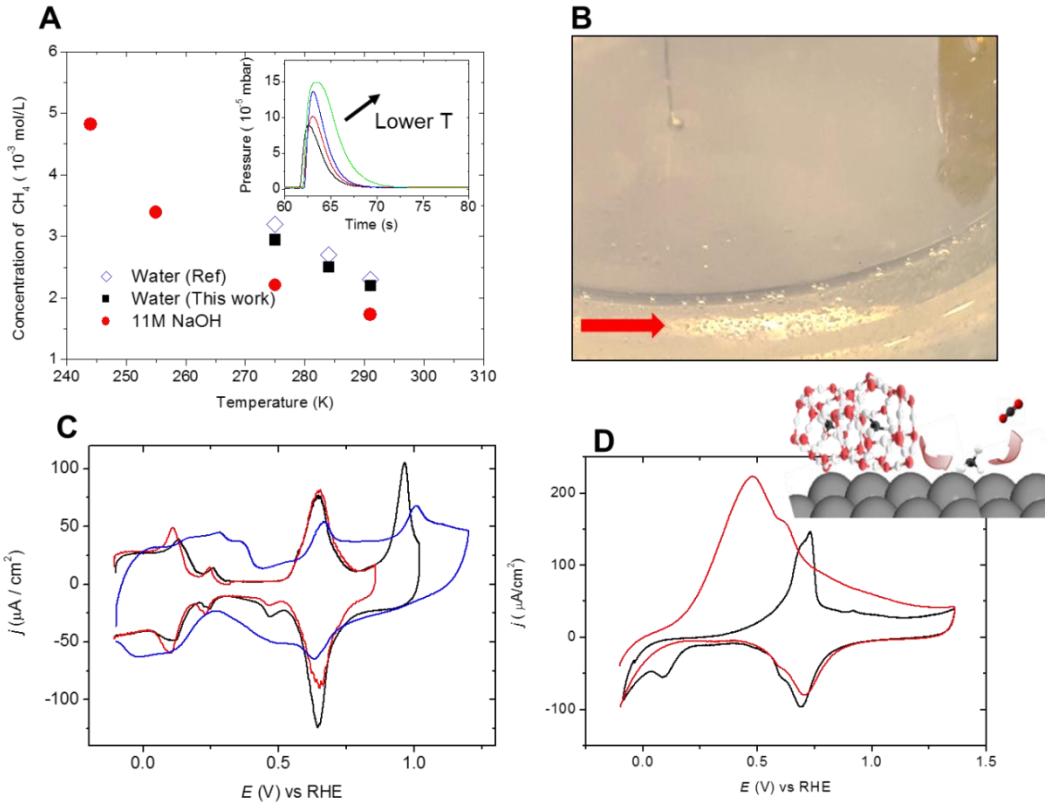

Figure 8. (A) Solubility curves of CH_4 as a function of the temperature in water and 11 m NaOH. The values of the solubility in water at different temperatures from Wiesenburg *et al.* and Duan *et al.* were included for validation of the method and proper comparison.[12, 39] Inset: Pressure vs time curves obtained from MS measurements at different temperatures. (B) Photograph of the opaque gel formed upon bubbling CH_4 in

11 m NaOH solution at -35 °C. (C) Voltammetric profile of Pt(111) electrode in 11 m NaOH in absence of CH_4 at -18 °C(red curve), in presence of CH_4 at -18 °C (black curve) and in presence of CH_4 at -38 °C (blue curve). Scan rate, υ=50 mV s^{-1} (D) Voltammetric profile of Pd electrode in 11 m NaOH at -38 °C in absence (black curve) and presence of CH_4 (red curve). Scan rate, υ=50 mV s^{-1}. Inset shows a schematic cartoon of the oxidation of CH_4 hydrate to CO_2.

The same observation is true for the oxidation of CH_4 on palladium electrodes, where the oxidation of methane only took place upon the formation of the gel at -38°C. As can be seen in Figure 8D, the onset of oxidation of CH_4 appears at 0.25 V, having a maximum at around 0.48 V vs RHE. Contrary to the observation on the platinum electrode, the reduction of palladium oxide is unaffected by the presence of CH_4 in solution. This indicates an absence of adsorbed poison species on the electrode and so a different reaction mechanism to platinum. Previous work in the gas phase and at higher temperatures has shown that oxygen-coated palladium surfaces favour the adsorption and dissociation of CH_4.[41] Consecutive scans, Figure 9A, show a decrease in the oxidation current of the methane on the Pd electrode, probably associated to the diffusion limitation of the gas towards the electrode through the viscous slurry. The oxidation of methane on Au(111) was also evaluated, however no oxidation was observed at any temperature, Figure S12.

2.3.1. Product characterization of the electrochemical reduction of CO_2 in brines

Long-term electrolysis was performed in other to determine the oxidation products of the CH_4 on Pt and Pd electrodes. During electrolysis the gas products were followed for a duration of 10 minutes using the modified OLEMS setup and liquids samples were collected after 5 and 10 min. The current transients, Figure 9B, showed a fast decrease in the current, reaching a plateau after 2 min. This is probably associated to the limited diffusion of the CH_4

to the surface, as observed in the cyclic voltammetry although the formation of poisonous species, which block active sites at the surface of the electrode, cannot be disregarded. No gas products were detected during the electrolysis, however if CO_2 was formed, due to the highly alkaline media, the formation of carbonate is expected. The qualitative analysis of the liquid products was performed by NMR shown in Figure 9C . Methanol and formic acid were the main liquid products observed.

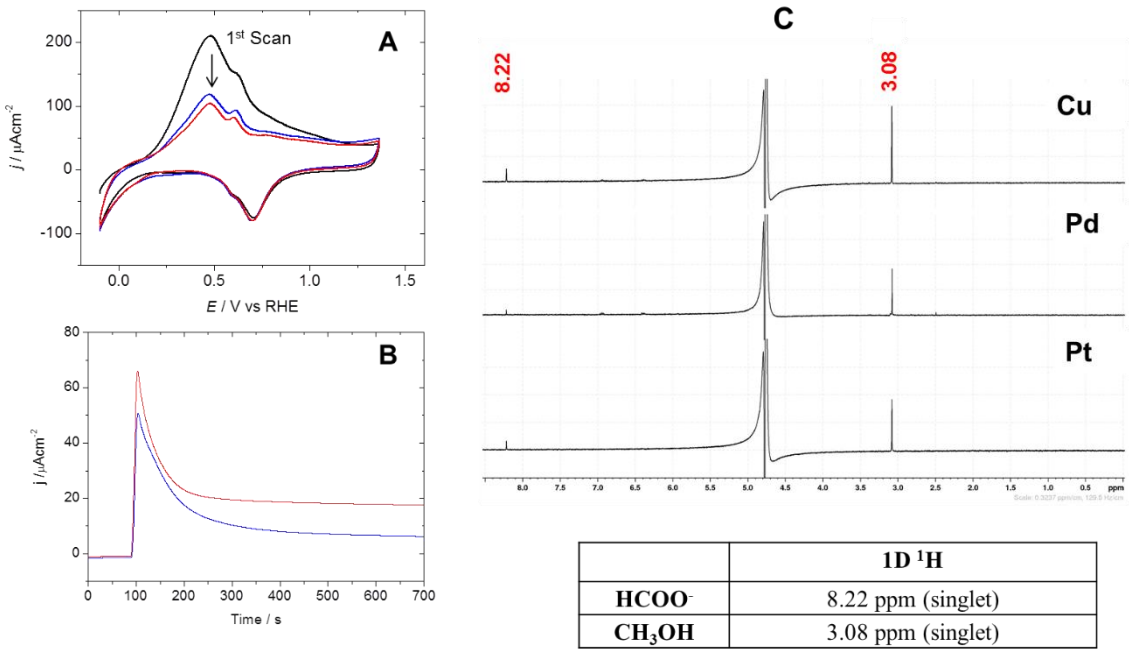

	1D ^{1}H
$HCOO^-$	8.22 ppm (singlet)
CH_3OH	3.08 ppm (singlet)

Figure 9. (A) Voltammetric profiles of consecutive scans, scan 1 (black curve) to scan 3 (red curve), of a Pd polyoriented electrode in 11 m NaOH at -35 °C in presence of CH_4. Scan rate, υ= 50 mV/s. (B) Current transients at 0.5 V vs RHE recorded on Pt(111) (blue curve) and Pd(polycrystalline) (red curve) electrodes in 11 m NaOH in presence of CH_4 at -38 °C. (C) 1D ^{1}H NMR spectrum recorded at 400 MHz for liquid samples collected after 20 min of electrolysis at 0.5 V vs RHE in CH_4-saturated solution of 10 m NaOH on (A) Cu(111), (B) Pd(polycrystalline), (C) Pt. The table includes NMR chemical shifts and multiplicities for the different products of CH_4 oxidation in 10 m NaOH found in the 1D ^{1}H spectra.

3. Conclusions

The use of brines as electrolytes is an efficient route to perform electrochemistry experiments at low temperatures. The large decrease in temperature greatly increases the solubility of non-polar gases such as CO_2 and CH_4, opening the door to new routes of electrocatalysis.

It was found that in brines of NaOH, KOH and $Mg(ClO_4)_2$ at low temperatures, the HER is hindered due to the formation of rigid ice-like structures at the interface between the electrode and electrolyte. In $Mg(ClO_4)_2$ brines at low temperatures, the HER from the water pathway competes with CO_2 reduction on a copper electrode at high overpotentials. At low overpotentials the water reduction to H_2, where the proton reduction reaction is a diffusion-limited process, hardly influences the reduction of CO_2 under mass transport conditions. Water reduction appears to be a slower process as the temperature decreases in comparison with the HER from protons. The combination of the high CO_2 concentration in solution and the decrease in the competitive HER results in a change in the product selectivity.

The electrochemical oxidation of CH_4 in NaOH brines was observed on Pt and Pd electrodes at temperatures below -35°C and upon the formation of a gel/slurry type solution. Small amounts of CO_2 were observed but the precise quantification of the products is not possible with the available techniques.

These systems open wide the door to many electrochemical applications in aqueous media where the reactions of interest are limited by the low solubility of the reactant species at high temperature or are limited by the HER.

We believe that a fundamental understanding, including modelling, of the formation of ice-like structures in these brines at the catalyst interface is very important and needs to be further explored.[42] In addition, further optimisation of the parameters of gas pressure,

temperature and composition of the electrolyte will allow the implementation of these systems in electrocatalysis.

In addition, our results provide an alternative explanation for the discovery of organic molecules on Mars.[43] The presence of small organic molecules such as CH_4 could be the result of the photochemical hydrogenation of CO_2, from the CO_2-saturated aqueous brines,[6e] catalysed by metal oxide semiconductors present in the Mars soil.[44] It is therefore relevant to extend these studies to photoelectrochemical systems and to those metals and metal oxides present on Mars, in order to complement this research.

4. Experimental Methods

The working electrodes used in this work were: Cu(111), Au(111), Pt(111) and Pt(100) bead type single crystal electrodes from (icryst) and a Pd disk (Alfa Aesar, 99.995%). Prior to each experiment, the Cu electrodes were prepared as described in reference.[45] The Au and Pt electrodes were prepared according to references.[46] The palladium working electrode was polished to a mirror finish using 1 μm diamond paste and then sonicated in Milli-Q water. The uncompensated solution resistance was measured as a function of the temperature using the positive feedback mode of the potentiostat and all voltammetries have been corrected by the Ohmic drop.

In the experiments, a high surface area gold wire or a high surface area Pt wire was used as a counter electrode accordingly and Hg/HgO was used as a reference electrode. All potentials are referenced to reversible hydrogen electrode, RHE. Electrochemical measurements were performed with an Autolab PGSTAT12.

Electrolyte solutions were prepared with high purity reagents (Sigma-Aldrich, KOH ≥85 %, NaOH ≥ 99%, Fischer Scientific, $Mg(ClO_4)_2.6H_2O$ Sigma-Aldrich 99%, K_2CO_3 ≥99%) and ultra-pure water (Elga PureUltra, 18.2 MΩ cm^{-1}, 1 ppb total organic carbon). Electrolytes

were purged with argon (Ar, N66), or saturated with methane (BOC, Research Grade) or CO_2 (BOC, Research Grade) for at least 20 minutes prior to the corresponding experiment. Details on calibration and experimental setup used for the determination of the solubility of the gases are included in the supporting information. The temperature control experiments were performed by immersing the electrochemical cell in a cooling medium of 1:1 glycerol:water and cooled to temperature using an HUBER TC45E-F immersion cooler. To accurately control the temperature of the electrolyte without contaminating the electrolyte inside the cell, the temperature was measured in a "shadow beaker" with a similar volume and placed next to the electrochemical cell inside the ice bath. The temperature was measured using a digital thermometer. In a control experiment, the temperature of the solution inside the cell and of the ghost beaker were measured simultaneously to ensure that the cell and the shadow beaker were in thermal equilibrium.

Further details on the gas analysis, Figure S13, and product characterisation and quantification can be found in the supporting information.

AUTHORS CONTRIBUTIONS

P.R conceived the experiments. The electrochemical experiments and product characterisation by mass spectrometry experiments were performed by E.S, A.K and P.R. NMR characterisation and analyses was performed by E.S and C.L.D. All authors contributed to the analysis of the results, discussion, writing and revision of the manuscript. All authors have given approval to the final version of the manuscript.

SUPPORTING INFORMATION

The supporting information includes complimentary experimental methods; product characterisation by mass spectroscopy and NMR; determination of gas solubility; electrochemical measurements on Pt(111) in $Mg(ClO_4)_2$, on polycrystalline Pd in 10 m KOH and on Au(111) in 11m NaOH; GC showing purity of CH_4

ACKNOWLEDGMENTS

ES acknowledges the University of Birmingham and the EPSRC Centre for Doctoral Training in Carbon Capture and Storage and Cleaner Fossil Energy for financial support through Ph.D. scholarships at the School of Chemistry. AK acknowledges the University of Birmingham for financial support through Ph.D. scholarships at the School of Chemistry. P.R. acknowledges the University of Birmingham for financial support .The authors would also like to acknowledge the reviewers of the manuscript that, during the revision process, suggested including a discussion regarding to mass transport which resulted in the preparation of the HMRDE experiments and analysis.

References

1. Davy, H., I. The Bakerian Lecture. On Some of the Combinations of Oxymuriatic Gas and Oxygene, and on the Chemical Relations of These Principles, to Inflammable Bodies. Philosophical Transactions of the Royal Society of London 1811, 101, 1-35.

2. Sloan Jr, E. D., Fundamental Principles and Applications of Natural Gas Hydrates. Nature 2003, 426, 353.

3. Sloan, E. D., Gas Hydrates: Review of Physical/Chemical Properties. Energy Fuels 1998, 12 (2), 191-196.

4. (a) C.A.Koh, E. D. Sloan, Clathrate hydrtaes of Natural Gases. Third Edition ed.; CRC Press: Boca Raton, Fl, USA, 2008; pp 22 (b) Koh, C. A.; Sloan, E. D.; Sum, A. K.; Wu, D. T., Fundamentals and Applications of Gas Hydrates. Annu. Rev. Chem. Biomol. Eng. 2011, 2 (1), 237-257.

5. Hecht, M. H.; Kounaves, S. P.; Quinn, R. C.; West, S. J.; Young, S. M. M.; Ming, D. W.; Catling, D. C.; Clark, B. C.; Boynton, W. V.; Hoffman, J.; DeFlores, L. P.; Gospodinova,

K.; Kapit, J.; Smith, P. H., Detection of Perchlorate and the Soluble Chemistry of Martian Soil at the Phoenix Lander Site. Science 2009, 325 (5936), 64-67.

6. (a) Safi, E.; Thompson, S. P.; Evans, A.; Day, S. J.; Murray, C. A.; Parker, J. E.; Baker, A. R.; Oliveira, J. M.; van Loon, J. T., Properties of CO2 Clathrate Hydrates Formed in the Presence of MgSO4 Solutions With Implications for Icy Moons. A&A 2017, 600, A88; (b) Martínez, G. M.; Renno, N. O., Water and Brines on Mars: Current Evidence and Implications for MSL. Space Sci. Rev., 2013, 175 (1), 29-51; (c) Martínez, G. M.; Newman, C. N.; De Vicente-Retortillo, A.; Fischer, E.; Renno, N. O.; Richardson, M. I.; Fairén, A. G.; Genzer, M.; Guzewich, S. D.; Haberle, R. M.; Harri, A.-M.; Kemppinen, O.; Lemmon, M. T.; Smith, M. D.; de la Torre-Juárez, M.; Vasavada, A. R., The Modern Near-Surface Martian Climate: A Review of In-situ Meteorological Data From Viking to Curiosity. Space Sci. Rev., 2017, 212 (1), 295-338; (d) Marion, G. M.; Catling, D. C.; Zahnle, K. J.; Claire, M. W., Modeling Aqueous Perchlorate Chemistries With Applications to Mars. Icarus 2010, 207 (2), 675-685; (e) Quinn, R. C.; Chittenden, J. D..; Kounaves, S. P.; Hecht, M. H., The oxidation-Reduction Potential of Aqueous Soil Solutions at the Mars Phoenix Landing Site. Geophys. Res. Lett., 2011, 38 (14).

7. (a) Onstott, T. C.; McGown, D.; Kessler, J.; Lollar, B. S.; Lehmann, K. K.; Clifford, S. M., Martian CH4: Sources, Flux, and Detection. Astrobiology 2006, 6 (2), 377-395; (b) Webster, C. R.; Mahaffy, P. R.; Atreya, S. K.; Moores, J. E.; Flesch, G. J.; Malespin, C.; McKay, C. P.; Martinez, G.; Smith, C. L.; Martin-Torres, J.; Gomez-Elvira, J.; Zorzano, M.-P.; Wong, M. H.; Trainer, M. G.; Steele, A.; Archer, D.; Sutter, B.; Coll, P. J.; Freissinet, C.; Meslin, P.-Y.; Gough, R. V.; House, C. H.; Pavlov, A.; Eigenbrode, J. L.; Glavin, D. P.; Pearson, J. C.; Keymeulen, D.; Christensen, L. E.; Schwenzer, S. P.; Navarro-Gonzalez, R.; Pla-García, J.; Rafkin, S. C. R.; Vicente-Retortillo, Á.; Kahanpää, H.; Viudez-Moreiras, D.; Smith, M. D.; Harri, A.-M.; Genzer, M.; Hassler, D. M.; Lemmon, M.; Crisp, J.; Sander, S.

P.; Zurek, R. W.; Vasavada, A. R., Background Levels of Methane in Mars' Atmosphere Show Strong Seasonal Variations. Science 2018, 360 (6393), 1093-1096.

8. Muscatello, A.; Santiago-Maldonado, E., Mars In Situ Resource Utilization Technology Evaluation; US, 2012, pp 1-13.

9. Duan, C.; Kee, R.; Zhu, H.; Sullivan, N.; Zhu, L.; Bian, L.; Jennings, D.; O'Hayre, R., Highly Efficient Reversible Protonic Ceramic Electrochemical Cells for Power Generation and Fuel Production. Nat. Energy, 2019, 4 (3), 230-240.

10. Mimachi, H.; Takahashi, M.; Takeya, S.; Gotoh, Y.; Yoneyama, A.; Hyodo, K.; Takeda, T.; Murayama, T., Effect of Long-Term Storage and Thermal History on the Gas Content of Natural Gas Hydrate Pellets under Ambient Pressure. Energy Fuels 2015, 29 (8), 4827-4834.

11. (a) Conway, B. E.; Salomon, M., Studies on the Hydrogen Evolution Reaction Down to —150°C and the Role of Proton Tunneling. J. Chem. Phys. 1964, 41 (10), 3169-3177; (b) Florit, M. I.; Arvia, A. J., The Voltammetric Behaviour of H and O Adatoms in the 189–292 K Range on Platinum in HClO4 • 5.5 H2O And H2SO4 • 12H2O. J. Electroanal. Chem. 1992, 339 (1), 281-297; (c) Safford, L. K.; Weaver, M. J., The Evaluation of Rate Constants for Rapid Electrode Reactions Using Microelectrode Voltammetry: Virtues of Measurements at Lower Temperatures. J. Electroanal. Chem. 1992, 331 (1), 857-876; (d) Frese, U.; Stimming, U., Hydrogen Evolution on Copper, Silver and Gold Electrodes in Aqueous Perchloric Acid 130 to 300 K. J. Electroanal. Chem. Interfacial Electrochem. 1986, 198 (2), 409-416.

12. Wiesenburg, D. A.; Guinasso, N. L., Equilibrium Solubilities of Methane, Carbon Monoxide, and Hydrogen in Water and Sea Water. J. Chem. Eng. Data 1979, 24 (4), 356-360.

13. Sanders, G. B. *In-Situ Resource Utilization (ISRU) Planning and Update*; National Aeronautics and Space Administration: Presentation to the NAC Technology, Innovation, and Engineering Committee Meeting. https://www.nasa.gov/sites/default/files/atoms/files/nac_tie_december_2018_gsanders_isru.pdf, 2018.

14. Florit, M. I.; Martins, M. E.; Arvia, A. J., Comparative Voltammetric Behaviour of H- and O-Atoms on a Pt Electrode in Sulphuric Acid Solutions Within the 293 K to 233 K Range. J. Electroanal. Chem. Interfacial Electrochem., 1989, 269 (1), 209-216.

15. deBethune, A. J.; Licht, T. S.; Swendeman, N., The Temperature Coefficients of Electrode Potentials. J. Electrochem. Soc., 1959, 106 (7), 616.

16. Markovic, N. M.; Schmidt, T. J.; Grgur, B. N.; Gasteiger, H. A.; Ross Jr, P. N.; Behm, R. J., The Effect of Temperature on the Surface Process at the Pt(111)-Liquid Inteface: Hydrogen Adsorption, Oxide Formation and CO Oxidation. J. Phys. Chem. B 1999, 103, 8568-8577.

17. Frese, U.; Iwasita, T.; Schmickler, W.; Stimming, U., Hydrogen Evolution in Liquid and Frozen Aqueous Electrolyte. J. Phys. Chem., 1985, 89 (7), 1059-1062.

18. Tielrooij, K. J.; Garcia-Araez, N.; Bonn, M.; Bakker, H. J., Cooperativity in Ion Hydration. Science 2010, 328 (5981), 1006-1009.

19. (a) Conway, B. E.; Bai, L., State of Adsorption and Coverage by Overpotential-Deposited H in the H2 Evolution Reaction at Au and Pt. Electrochim. Acta 1986, 31 (8), 1013-1024; (b) Schuldiner, S., Hydrogen Overvoltage on Bright Platinum: II . pH and Salt Effects in Acid, Neutral, and Alkaline Solutions. J. Electrochem. Soc. 1954, 101 (8), 426-432; (c) Sheng, W.; Gasteiger, H. A.; Shao-Horn, Y., Hydrogen Oxidation and Evolution Reaction Kinetics on Platinum: Acid vs Alkaline Electrolytes. J. Electrochem. Soc. 2010, 157

(11), B1529-B1536.(d) Schmidt,T.J; Ross Jr., P.N.; Markovic, N.M., Temperature Dependent Surface Electrochemistry on Pt Single Crystals in Alkaline Electrolytes: Part 2. The Hydrogen Evolution/Oxidation Reaction. J. Electroanal. Chem. 2002, 524 – 525, 252 – 260.

20. Ledezma-Yanez, I.; Wallace, W. D. Z.; Sebastián-Pascual, P.; Climent, V.; Feliu, J. M.; Koper, M. T. M., Interfacial Water Reorganization as a pH-Dependent Descriptor of the Hydrogen Evolution Rate on Platinum Electrodes. Nat. Energy 2017, 2, 17031.

21. Bai, D.; Chen, G.; Zhang, X.; Sum, A. K.; Wang, W., How Properties of Solid Surfaces Modulate the Nucleation of Gas Hydrate. Sci. Rep. 2015, 5, 12747.

22. Opallo, M.; Prokopowicz, A., Electrochemical Hydrogen Evolution in Hydroxide Hydrate Down to 110 K. Electrochem. Commun. 2000, 2 (1), 23-26.

23. Chen, X.; McCrum, I. T.; Schwarz K. A.; Janik, M. J.; Koper, M. T. M;, Co-adsorption of Cations as the Cause of the Apparent pH Dependence of Hydrogen Adsorption on a Stepped Platinum Single-Crystal Electrode. Angew. Chem. Int. Ed. 2017, 56 (47), 15025-15029.

24. Zhang, W.-S.; Zhang, X.-W.; Zhao, X.-G., Voltammograms of Thin Layer Pd|H(D) Electrodes in the Coexistence of α and β Phases. J. Electroanal. Chem. 1998, 458 (1), 107-112.

25. (a) Zhou, F.; Li, H.; Fournier, M.; MacFarlane D. R., Electrocatalytic CO2 Reduction to Formate at Low Overpotentials on Electrodeposited Pd Films: Stabilized Performance by Suppression of CO Formation. ChemSusChem 2017, 10 (7), 1509-1516; (b) Humphrey, J. J. L.; Plana, D.; Celorrio, V.; Sadasivan, S.; Tooze, R. P.; Rodríguez, P.; Fermín, D. J., Electrochemical Reduction of Carbon Dioxide at Gold-Palladium Core–Shell Nanoparticles: Product Distribution versus Shell Thickness. Chemcatchem 2016, 8 (5), 952-960.

26. Duan, Z.; Sun, R., An Improved Model Calculating CO2 Solubility in Pure Water and Aqueous NaCl Solutions From 273 to 533 K and From 0 to 2000 bar. Chem. Geol. 2003, 193 (3), 257-271.

27. Kuhl, K. P.; Cave, E. R.; Abram, D. N.; Jaramillo, T. F., New Insights Into the Electrochemical Reduction of Carbon Dioxide on Metallic Copper Surfaces. Energy Environ. Sci. 2012, 5 (5), 7050-7059.

28. Min, X.; Kanan, M. W., Pd-Catalyzed Electrohydrogenation of Carbon Dioxide to Formate: High Mass Activity at Low Overpotential and Identification of the Deactivation Pathway. J. Am. Chem. Soc. 2015, 137 (14), 4701-4708.

29. (a) Rodriguez, P.; Feliu, J. M.; Koper, M. T. M., Unusual Adsorption State of Carbon monoxide on Single-Crystalline Gold Electrodes in Alkaline Media. Electrochem. Commun. 2009, 11 (6), 1105-1108; (b) Rodriguez, P.; Garcia-Araez, N.; Koper, M. T. M., Self-Promotion Mechanism for CO Electrooxidation on Gold. Phys. Chem. Chem. Phys 2010, 12 (32), 9373-9380; (c) Rodriguez, P.; Garcia-Araez, N.; Koverga, A.; Frank, S.; Koper, M. T. M., CO Electroxidation on Gold in Alkaline Media: A Combined Electrochemical, Spectroscopic, and DFT Study. Langmuir 2010, 26 (14), 12425-12432.

30. Ooka, H.; Figueiredo, M. C.; Koper, M. T. M., Competition Between Hydrogen Evolution and Carbon Dioxide Reduction on Copper Electrodes in Mildly Acidic Media. Langmuir 2017, 33 (37), 9307-9313.

31. Ke, K.; Hiroshima, K.; Kamitaka, Y.; Hatanaka, T.; Morimoto, Y., An Accurate Evaluation for the Activity of Nano-Sized Electrocatalysts by a Thin-Film Rotating Disk Electrode: Oxygen Reduction on Pt/C. Electrochim. Acta 2012, 72, 120-128.

32. Lee, C. W.; Cho, N. H.; Im, S. W.; Jee, M. S.; Hwang, Y. J.; Min, B. K.; Nam, K. T., New Challenges of Electrokinetic Studies in Investigating the Reaction Mechanism of Electrochemical CO2 Reduction. J. Mater. Chem. A 2018, 6 (29), 14043-14057.

33. Ahn, S. T.; Abu-Baker, I.; Palmore, G. T. R., Electroreduction of CO2 on Polycrystalline Copper: Effect of Temperature on Product Selectivity. Catal. Today 2017, 288, 24-29.

34. Wang, L.; Nitopi, S. A.; Bertheussen, E.; Orazov, M.; Morales-Guio, C. G.; Liu, X.; Higgins, D. C.; Chan, K.; Nørskov, J. K.; Hahn, C.; Jaramillo, T. F., Electrochemical Carbon Monoxide Reduction on Polycrystalline Copper: Effects of Potential, Pressure, and pH on Selectivity toward Multicarbon and Oxygenated Products. ACS Catal. 2018, 8 (8), 7445-7454.

35. (a) Lum, Y.; Yue, B.; Lobaccaro, P.; Bell, A. T.; Ager, J. W., Optimizing C–C Coupling on Oxide-Derived Copper Catalysts for Electrochemical CO2 Reduction. J. Phys. Chem. C 2017, 121 (26), 14191-14203; (b) Nitopi, S.; Bertheussen, E.; Scott, S. B.; Liu, X.; Engstfeld, A. K.; Horch, S.; Seger, B.; Stephens, I. E. L.; Chan, K.; Hahn, C.; Nørskov, J. K.; Jaramillo, T. F.; Chorkendorff, I., Progress and Perspectives of Electrochemical CO2 Reduction on Copper in Aqueous Electrolyte. Chem. Rev. 2019, 119 (12), 7610-7672.

36. (a) Liang, S.; Liang, D.; Wu, N.; Yi, L.; Hu, G., Molecular Mechanisms of Gas Diffusion in CO2 Hydrates. J. Phys. Chem. C 2016, 120 (30), 16298-16304; (b) Liang, S.; Liang, D.; Wu, N.; Yi, L.; Hu, G., Transient Translational and Rotational Water Defects in Gas Hydrates. J. Phys. Chem. C 2017, 121 (33), 17595-17602.

37. Luo, W.; Nie, X.; Janik, M. J.; Asthagiri, A., Facet Dependence of CO2 Reduction Paths on Cu Electrodes. ACS Catal. 2016, 6 (1), 219-229.

38. (a) Sohl, F.; Choukroun, M.; Kargel, J.; Kimura, J.; Pappalardo, R.; Vance, S.; Zolotov, M., Subsurface Water Oceans on Icy Satellites: Chemical Composition and Exchange Processes. Space Sci. Rev. 2010, 153 (1), 485-510; (b) Marion, G. M.; Kargel, J. S.; Catling, D. C.; Lunine, J. I., Modeling Nitrogen-Gas, -Liquid, -Solid Chemistries at Low Temperatures (173–298K) With Applications to Titan. Icarus 2014, 236, 1-8.

39. Duan, Z.; Møller, N.; Greenberg, J.; Weare, J. H., The Prediction of Methane Solubility in Natural Waters to High Ionic Strength From 0 to 250°C and From 0 to 1600 bar. Geochim. Cosmochim. Acta 1992, 56 (4), 1451-1460.

40. Gudmundsson, J. S.; Andersson, V.; Levik, O. I.; Mork, M., Hydrate Technology for Capturing Stranded Gas. Ann. N. Y. Acad. Sci. 2000, 912 (1), 403-410.

41. Hellman, A.; Resta, A.; Martin, N. M.; Gustafson, J.; Trinchero, A.; Carlsson, P. A.; Balmes, O.; Felici, R.; van Rijn, R.; Frenken, J. W. M.; Andersen, J. N.; Lundgren, E.; Grönbeck, H., The Active Phase of Palladium During Methane Oxidation. J. Phys. Chem. Lett 2012, 3 (6), 678-682.

42. Factorovich, M. H.; Molinero, V.; Scherlis, D. A., Hydrogen-Bond Heterogeneity Boosts Hydrophobicity of Solid Interfaces. J. Am. Chem. Soc. 2015, 137 (33), 10618-10623.

43. ten Kate, I. L., Organic molecules on Mars. Science 2018, 360 (6393), 1068-1069.

44. (a) Rieder, R.; Economou, T.; Wänke, H.; Turkevich, A.; Crisp, J.; Brückner, J.; Dreibus, G.; McSween, H. Y., The Chemical Composition of Martian Soil and Rocks Returned by the Mobile Alpha Proton X-ray Spectrometer: Preliminary Results from the X-ray Mode. Science 1997, 278 (5344), 1771-1774; (b) Bandfield, J. L.; Hamilton, V. E.; Christensen, P. R., A Global View of Martian Surface Compositions from MGS-TES. Science 2000, 287 (5458), 1626-1630.

45. Le Duff, C. S.; Lawrence, M. J.; Rodriguez, P., Role of the Adsorbed Oxygen Species in the Selective Electrochemical Reduction of CO2 to Alcohols and Carbonyls on Copper Electrodes. Angew. Chem., 2017, 129 (42), 13099-13104.

46. (a) Clavilier, J.; Armand, D.; Sun, S. G.; Petit, M., Electrochemical Adsorption Behaviour of Platinum Stepped Surfaces in Sulphuric Acid Solutions. J. Electroanal. Chem. Interfacial Electrochem. 1986, 205 (1–2), 267-277; (b) Edens, G. J.; Hamelin, A.; Weaver, M. J., Mechanism of Carbon Monoxide Electrooxidation on Monocrystalline Gold Surfaces: Identification of a Hydroxycarbonyl Intermediate. J. Phys. Chem. 1996, 100 (6), 2322-2329.

COMPETING INTEREST

The authors declare no competing interests.

TOC.